EMCO-based Optimal Layout Design of Hybrid Wind-wave Energy Converters Array

Bo Yang, Jinhang Duan, Yunfeng Yan, Bingqiang Liu, Jianxiang Huang, Lin Jiang, and Rui Han

***Abstract*—Marine renewable energy, combining wave energy converters (WECs) and floating wind turbines (FWTs) into hybrid wave-wind energy converters (HWWECs), garners significant global interest. HWWECs offer potential cost reductions, increased power generation, and enhanced system stability. The absorption power of high wind energy sites is primarily influenced by the complex hydrodynamic interactions among floating bodies, which are closely related to the location and wind-wave environment of high wind energy sites. To delve into the positive interactions among HWWECs, this paper proposes a HWWEC array optimization strategy based on the artificial ecosystem optimization-manta ray foraging optimization coordinated optimizer (EMCO). In EMCO, the decomposition operator of artificial ecosystem optimization (AEO) and the flipping-dipper foraging operator of manta ray foraging optimization coordinated (MRFO) cooperate dynamically to effectively balance local exploitation and global exploration. To validate the effectiveness of EMCO, experiments were conducted in scenarios with 3, 5, 8, and 20 HWWECs, and compared with five typical algorithms. Experimental results demonstrate the existence of multiple optimal solutions for HWWEC arrays. EMCO achieves maximum total absorption power and exhibits good stability. Notably, EMCO enhances the *q*-factor values of HWWECs across four scales: 1.0478, 1.0586, 1.0612, and 0.9965, respectively.**

***Index Terms*—Marine renewable energy, hybrid wind-wave energy converter, layout optimization, coordinating optimizer.**

Received: November 5, 2023
Accepted: June 1, 2024
Published Online: September 1, 2024

Bo Yang, Jinhang Duan, Bingqiang Liu are with the Faculty of Electric Power Engineering, Kunming University of Science and Technology, Kunming 650500, China (e-mail: yangbo_ac@outlook.com; 2972092338@qq.com; 2451250809@qq.com).

Yunfeng Yan (corresponding author) is with the College of Electrical Engineering, Zhejiang University, Hangzhou 310027, China (e-mail: Yunfengyan123@outlook.com).

Jianxiang Huang is with the Company of Kunming Bureau of CSG EHV Transmission Company, Kunming 650217, China (e-mail: 3341370580@qq.com).

Lin Jiang is with the School of Electrical Engineering and Electronics, University of Liverpool, Liverpool L69 3GJ, UK (e-mail: l.jiang@liv.ac.uk).

Rui Han is with the Company of Electric Power Science Research Institute, State Grid Zhejiang Electric Power Company Ltd., Hangzhou 310014, China (e-mail:1648586204@qq.com).

DOI: 10.23919/PCMP.2023.000129

NOMENCLATURE

A. Abbreviations

AEO	artificial ecosystem optimization
AEP	annual energy production
ART	adaptive resonance theory
CGO	chaos game optimization
FWT	floating wind turbine
GWO	grey wolf optimizer
HBA	honey badger algorithm
HWWEC	hybrid wind-wave energy converter
MRFO	manta ray foraging optimization
MhAs	meta-heuristic algorithms
OWF	offshore wind farm
PTO	power take-off
PV	photovoltaic
RES	renewable energy source
SFC	semisubmersible flap combination
STC	spare torus combination
WEC	wave energy converter
WT	wind turbine

B. Variables

A_{wheel}	swept area of FWT
$\boldsymbol{A}(\omega)$	additional mass matrices
a^{t}	linear weight coefficient
$\boldsymbol{\alpha}$	weight coefficient
α_{w}	axial induction factor
$\boldsymbol{B}'$	quadratic viscous damping coefficient
$\boldsymbol{\beta}$	weight coefficient
$\boldsymbol{B}_{\text{pto},\Sigma}$	damping block-matrices
$\boldsymbol{B}(\omega)$	damping coefficient matrices
C_{drag}	wind drag coefficient
C	consumer operator
$\boldsymbol{D}$	decentralized factor
F^{FWT}	wave load
F_{wind}	wind load
F_{wave}	wave load
F_{pto}	PTO system load
$F_{\text{w-drag}}$	wind wheel thrust load

F_{exc}	wave forces of excitation
F_{rad}	wave forces of radiation
g	gravitational acceleration
$\boldsymbol{K}_{\text{pto},\Sigma}$	stiffness block-matrices
$P_{\text{FWT},\Sigma}$	absorbed power of FWTs
$P_{\text{WEC},\Sigma}$	absorbed power of WECs
P_{Σ}	total absorbed power of a HWWECs array
P_0	absorbed power of a single HWWEC
P_j	absorbed power of the *j*th HWWEC in an array
P_{p}	yaw adjustment parameter
$\boldsymbol{R}$	restoring coefficient matrices
S	somersault factor
v_{w}	effective wind speed
$\boldsymbol{x}$	displacement vector
$\dot{\boldsymbol{x}}$	velocity vector
$\ddot{\boldsymbol{x}}$	acceleration vector
ρ_{a}	air density
ρ_{β}	water density
η_{w}	correction coefficient
γ_{w}	yaw angle of the WT
θ	wave propagation angle

I. Introduction

In the past few decades, environmental issues such as global warming and sea-level rise are becoming much more severe than before, whilst global demand for electrical energy is dramatically increasing [1], [2]. Nevertheless, traditional fossil fuels, e.g., coal, oil, and natural gases are facing ever-increasing depletion [3]. Therefore, with the motivation to prevent environmental degradation and reform energy structure, renewable energy sources (RESs) have been widely developed and utilized all over the world, e.g., solar, wind, ocean energies, etc. [4]–[6]. Marine renewable energy has become a strategic resource to implement technology reserves internationally thanks to its great location conditions and development potential. At present, marine renewable energy can be mainly subdivided into ocean current energy, offshore wind energy, tidal energy, ocean thermal energy, and wave energy [7], [8]. Among them, offshore wind energy is widely developed and utilized, with wind farms scaled up to 1000 MW [9]. Compared with onshore wind turbines, offshore wind turbines (WTs) can usually receive higher and less turbulent wind speeds [10]. Meanwhile, they can provide stable output power without mechanical noise restrictions. Hence, the annual energy production (AEP) of offshore wind farms (OWFs) is relatively higher. Their electricity production increased from 56 TWh to 67 TWh in 2018. According to the International Energy Agency sustainable development scenario, the power generation of OWFs will reach 308 TWh and 606 TWh in 2025 and 2030 respectively [11]. Furthermore, ocean wave energy is also a crucial resource in the offshore environment. It has become a common focus around the world due to its high energy density and wide distribution [12], [13]. Thus far, wave energy conversion technology has been not mature enough and still in the development stage. However, it has huge development potential for contribution to RES harnessing. Specifically, about 1 TW of power potential can be generated by wave energy available along the world's coasts, which might even reach up to 10 TW while the open ocean is considered [14], [15]. The power production of ocean waves might approximately reach 93 TWh per annum [16].

Since the natural correlation between sea wind and wave, scientific integration of floating wind turbine (FWT) and wave energy converter (WEC) can become a promising technology. A hybrid wind-wave energy converter (HWWEC) can simultaneously capture energy from wind and wave, which greatly reduces the downtime period of OWFs [17]. Especially, the power take-off (PTO) can convert wave energy captured by WEC and buoy platforms into electrical energy. Afterwards, the electricity generated by HWWEC is transmitted to the land via submarine cables. Meanwhile, the ocean utilization area and installation costs can be significantly saved by sharing infrastructure for electrical systems, mooring systems, and other common components [18], [19]. In recent years, various HWWEC systems have been proposed, upon which the most representative and influential HWWEC systems are mainly spare torus combination (STC) and semi-submersible flap combination (SFC) proposed by marine renewable integrated application platform project funded by the European Union [20]–[22]. Reference [23] indicated that a colocated offshore wind-wave farm has an increment of 3.4% in the annual energy yield compared with a standalone OWF. In addition, the generation ability of WECs in offshore hybrid wind-wave farms was comprehensively analyzed and evaluated in the literature [9]. For the dynamic analysis of HWWEC, reference [24] established the wind-wave coupled hydrodynamic model and studied the feasibility of HWWEC by aero-servo-hydro-elastic simulation tool. Besides, many factors can impact the power performance and motion response of HWWEC, e.g., WEC types, WEC shape, WT types, WT size, and wind-wave conditions, etc. Reference [25] proposed HWWEC consisting of a monopile-type WT and a heave-type WEC, and its hydrodynamic responses were deeply researched by numerical simulations. Meanwhile, a concept of HWWEC combined with a 5 MW semi-submersible FWT and a torus-type WEC was innovated

in reference [26], where the effect of different WEC shapes on motion response and power performance was investigated in detail.

Moreover, partial HWWECs are generally installed on the sea in the form of arrays or farms to realize large electricity production and grid integration. However, unlike photovoltaic (PV) arrays, there are sophisticated interactions among floaters in HWWECs array, which might be constructive or destructive to the total absorbed power [27], [28]. These interactions rely on the distances and orientations among floaters [29], [30]. In fact, from the analysis of WECs arrays' power characteristics [31]–[34], the absorbed power of HWWECs array might be much higher than that generated by the same number of dividual HWWECs, which is strongly relevant to the layout of HWWECs array. Therefore, it is crucial to adequately exploit the constructive interaction of floaters in HWWECs array for improving its energy conversion rate.

Needless to say, optimization of HWWECs array layout is a tricky problem because of the complex wind-wave environments and interactions in HWWECs farm. So far, various methods have been put forward to realize the optimization of WECs array layout, e.g., machine learning methods, mathematical methods, and meta-heuristic algorithms (MhAs) [13]. Nevertheless, to authors' best understanding and knowledge, the issue layout optimization of HWWECs array has been rarely studied in the present work. Inspiringly, a novel concept of HWWEC is proposed in this paper. As shown in Fig. 1, it consists of FWT (Vestas V27–225 kW WT [35]), three-tether WEC [31], PTO and mooring systems. FWT is flexible, it can be disassembled and moved to a suitable location, so as to capture offshore wind energy. And wave energy can be captured by WEC and floating platform from many directions. By using cable and pulley mechanism, the WEC can work in high efficiency by capturing wave energy in both surge and heave mode even though there is changing water level. Then, the electricity generated by HWWEC is transported by submarine cables to onshore converter stations. As mentioned above, MhAs are widely utilized in many optimizations working with the strong nonlinearity. However, the model of HWWEC array contains many complex modules, e.g., sea state simulation and hydrodynamic interaction module between buoys, etc. Most algorithms with complex mechanisms are not suitable for solving such optimization problems due to the computational cost. Therefore, it is urgent to find a method with a strong optimization ability and a simple mechanism to optimize the layout of HWWEC array. Based on the inspiration of artificial ecosystem optimization (AEO) [36] and manta ray foraging optimization (MRFO) [37], a novel AEO-MRFO coordinating optimizer (EMCO) is developed for layout optimization of HWWECs array in this work. EMCO has great experimental performance, simple structure, strong optimization ability, etc., which is a better scheme in various layout optimization methods of WEC array. The performances of EMCO are mainly assessed by two evaluation criteria including total absorbed power and q-factor for HWWECs farm. The key contributions of this paper can be summarized as follows:

1) A novel HWWEC consisting of a Vestas V27–225 kW WT and a three-tether WEC is originally proposed to capture energy from the wind and wave as much as possible. Meanwhile, the hydrodynamic model of HWWECs array is established.

2) In order to improve the placement of HWWEC in a wind-wave farm and maximize the absorbed power of HWWECs array, a novel coordinating optimizer named EMCO is proposed for layout optimization of HWWECs array.

3) Practical and specific performances of HWWECs array optimized by EMCO are comprehensively evaluated under four scenarios, e.g., 3-HWWEC, 5-HWWEC, 8-HWWEC, and 20-HWWEC farms, via a thorough comparison with that of five typical MhAs, i.e., AEO, MRFO, grey wolf optimizer (GWO), chaos game optimization (CGO) and honey badger algorithm (HBA).

The rest of this work is structured as follows. HWWECs array model is established in Section II. Section III and Section IV introduce the design of EMCO and the optimization of HWWECs array based on EMCO, in which the principle, framework, and execution process of EMCO are provided, respectively. In Section V, case studies and statistical analysis are carried out. Finally, the main conclusions and future developments are drawn in Section VI.

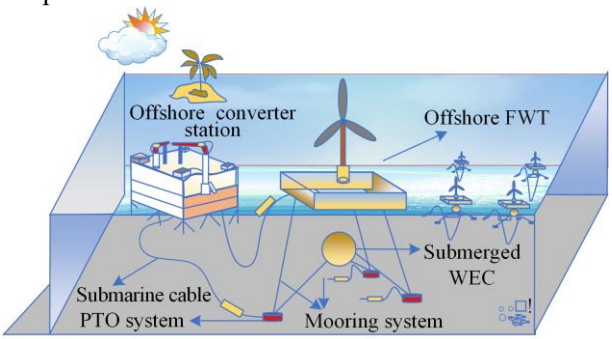

Fig. 1. A conceptual illustration of the HWWECs array.

II. Hybrid Wind-Wave Energy Converter Array Modelling

A. Dynamics Analysis

1) Floating Wind Turbine System

Considering the FWT as a particle, the total external loads acting on the FWT are mainly the aerodynamic load transmitted by the WT, wave load, and the load of mooring systems and PTO [24], [38]. Besides, there are two loads in aerodynamic load: wind wheel thrust $F_{\text{w-drag},i}$ and wind drag $F_{\text{w-drag}}$. And aerodynamic load of WT $F_{\text{wind}}(i)$ can be calculated by the blade element theory [39], [40]. Therefore, the motion of FWT can be described as:

$$\begin{cases} F_i^{\mathrm{FWT}} = F_{\mathrm{wind},i} + F_{\mathrm{wave},i} + F_{\mathrm{pto},i} \\ F_{\mathrm{wave},i} = F_{\mathrm{exc},i} + F_{\mathrm{rad},i} \\ F_{\mathrm{wind},i} = F_{\mathrm{w\text{-}drag},i} + F_{\mathrm{w\text{-}thrust},i} \\ F_{\mathrm{w\text{-}drag}} = \dfrac{1}{2}\rho_{\mathrm{a}} C_{\mathrm{drag}} A_{\mathrm{drag}} U_{\infty}^2 \\ P_{\mathrm{FWT}} = \displaystyle\sum_{i=1}^{N} \frac{1}{2}\rho_{\mathrm{a}} A_{\mathrm{wheel}} 4\alpha_{\mathrm{w}} \times \\ \qquad (1-\alpha_{\mathrm{w}})^2 \eta_{\mathrm{w}} (\cos\gamma_{\mathrm{w}})^{P_{\mathrm{p}}} v_{\mathrm{w}}^3 \end{cases} \tag{1}$$

where $F_{\mathrm{wind},i}$, $F_{\mathrm{wave},i}$, and $F_{\mathrm{pto},i}$ are acting on FWT loads by wind, wave, and PTO system; $F_{\mathrm{exc},i}$ and $F_{\mathrm{rad},i}$ are the wave forces of excitation and radiation; A_{drag} is the orthographic projection area above the waterplane of the tower and platform in the direction of incoming flow; U_{∞} is the upwind speed of the distant flow; ρ_{a} is the air density; C_{drag} is the wind drag coefficient; P_{FWT} is the power absorbed by WT from ocean wind energy; A_{wheel} is the swept area of WT; α_{w} is the axial induction factor; η_{w} is the correction coefficient; γ_{w} is the yaw angle of the WT; P_{p} is the yaw adjustment parameter; and v_{w} is the effective wind speed.

2) Wave Energy Converter System

Using the same method, two loads including wave load and PTO system load can be acting on the WEC. The hydrodynamic interactions among buoys are crucial elements in WEC performance. Based on the linear wave theory and potential flow theory, the dynamics equation of WEC can be described as follows [31]:

$$\begin{cases} \left((\boldsymbol{M}_{\mathrm{WEC}} + \boldsymbol{A}_{\mathrm{WEC}})(\omega)\mathrm{j}\omega + \boldsymbol{B}_{\Sigma}(\omega) - \dfrac{\boldsymbol{K}_{\mathrm{pto},\Sigma}}{\omega}\mathrm{j} + \boldsymbol{B}_{\mathrm{pto},\Sigma} \right) \hat{\boldsymbol{x}}_{\mathrm{WEC}} = \hat{F}_{\mathrm{exc},\Sigma} \\ P_{\mathrm{WEC}} = \dfrac{1}{4}(\hat{F}_{\mathrm{exc},\Sigma}^{*}\dot{\boldsymbol{x}}_{\Sigma} + \dot{\boldsymbol{x}}_{\Sigma}^{*}\hat{F}_{\mathrm{exc},\Sigma}) - \dfrac{1}{2}\dot{\boldsymbol{x}}_{\Sigma}^{*} B \dot{\boldsymbol{x}}_{\Sigma} \end{cases} \tag{2}$$

where $\boldsymbol{M}$ stands for the mass matrix; $\hat{\boldsymbol{x}}_{\mathrm{WEC}}$ is the generalized acceleration vector of WECs; the symbol "*" means the conjugate transpose; $\boldsymbol{A}_{\mathrm{WEC}}(\omega)$ and $\boldsymbol{B}_{\Sigma}(\omega)$ denote the added mass matrices and damping coefficient matrices, which express hydrodynamic interactions of buoys; P_{WEC} is the power absorbed by WEC from ocean wave energy; $\boldsymbol{K}_{\mathrm{pto},\Sigma}$ and $\boldsymbol{B}_{\mathrm{pto},\Sigma}$ represent the stiffness and damping block matrices of PTO systems, respectively.

3) Hybrid Wind-wave Energy Converter System

Firstly, Vestas V27–225 kW WT [35] and three-tether WEC [31] are chosen as the FWT system and WEC system of HWWEC respectively in this work. Meanwhile, the hydrodynamic performances of HWWECs can be simulated in the frequency domain by WAMIT, e.g., excitation force, added mass, wave-wind coupling terms, etc. At last, in order to simplify the interaction between HWWECs, just three dominant external forces which act on HWWECs are considered in this paper. The total external loads of HWWEC mainly include the load transmitted by WT, the wave load, and the load of the PTO acting on HWWEC by tethers. According to the linear potential flow theory [24], [41], the frequency domain equation of HWWEC's motion is given by

$$\begin{aligned} &-\omega^2 \left\{ M_{\mathrm{HWWEC}} + \boldsymbol{A}(\omega) \right\} \boldsymbol{X}(\omega) + \\ &i\omega B(\omega)\boldsymbol{X}(\omega) + R\boldsymbol{X}(\omega) = F_{\Sigma}(\omega) \end{aligned} \tag{3}$$

$$F_{\Sigma}(\omega) = F_{\mathrm{wind}}(\omega) + F_{\mathrm{wave}}(\omega) + F_{\mathrm{pto}}(\omega) \tag{4}$$

where $F_{\Sigma}(\omega)$ is the external force; M_{HWWEC} is the structural mass of HWWEC; $\boldsymbol{A}(\omega)$ and $\boldsymbol{X}(\omega)$ are the additional mass matrices and displacement vectors in the frequency domain; B and R are the damping coefficient and restoring coefficient; $F_{\mathrm{wind}}(\omega)$, $F_{\mathrm{wave}}(\omega)$ and $F_{\mathrm{pto}}(\omega)$ are the acting on HWWEC loads by wind, wave, and PTO system, respectively.

In order to further analyze the nonlinear effects between the HWWECs in the time domain, equation (3) can be extended as [24], [41].

$$\begin{aligned} &\left\{ M_{\mathrm{HWWEC}} + A(\infty) \right\} \ddot{x}(t) + B'\dot{x}|\dot{x}| + \\ &\int_0^t \boldsymbol{k}(t-\tau)x(\tau)\mathrm{d}\tau + Rx(t) = f(t,x,\dot{x}) \end{aligned} \tag{5}$$

where $A(\infty)$ is the added mass at infinite frequency; x, $\dot{x}$, and $\ddot{x}$ are the displacement, velocity, and acceleration in the time domain respectively; B' is the quadratic viscous damping coefficient; and $\boldsymbol{k}(\tau)$ is the velocity impulse function matrix.

B. Performance Index

Assume N is the total number of HWWECs in an array. After determining the wave and wind conditions, i.e., wave frequency, wave height, wind speed, and direction. In the frequency domain, the total power absorbed by a completed HWWECs array from ocean wind-wave can be calculated by

$$P_{\Sigma} = P_{\mathrm{WEC},\Sigma} + P_{\mathrm{FWT},\Sigma} \tag{6}$$

To evaluate the optimization quality of HWWECs array and compare the optimization effects among different HWWECs arrays, q-factor is referred to as the specific parameter to evaluate the performance of HWWECs array in this paper, which can be defined as

$$q = \frac{P_{\Sigma}}{NP_0} \tag{7}$$

where N is the number of the HWWECs; P_0 is the power absorbed of wind-wave energy captured by HWWEC when working alone.

The q-factor is initially used to evaluate the performance of WECs array and it can be greater than 1 in theory, which indicates a WEC in the array can absorb more energy than an individual device [42]–[44]. The q-factor shows the ratio of the absorbed power of

the HWWECs array compared to the absorbed power of the same number HWWECs in isolation.

III. DESIGN OF EMCO

A. Primal AEO

For AEO, the producer $x_1(t)$ updates its position through the decomposer position $x_n(t)$ in the current population and a random vector $\boldsymbol{x}_r$ within the search range [31], as follows:

$$a^{\mathrm{t}} = \left(1 - \frac{t}{t_{\max}}\right) r_1 \tag{8}$$

$$\boldsymbol{x}_r = \boldsymbol{r}(U_i^{\mathrm{b}} - L_i^{\mathrm{b}}) + L_i^{\mathrm{b}} \tag{9}$$

$$x_1(t+1) = (1-a)x_n(t) + a\boldsymbol{x}_r \tag{10}$$

where a^{t} is a linear weight coefficient; $t_{\max}$ is the maximum number of iterations; r_1 is a random parameter [0, 1]; $\boldsymbol{r}$ is a random vector that follows a uniform distribution in [0, 1]; L_i^{b} and U_i^{b} are the lower and upper limits of the searching domain; and n is the population size.

If consumer $x_i(t)$ is an herbivore, only the energy of the producer can flow to the herbivore, which yields

$$x_i(t+1) = x_i(t) + C\left[x_i(t) - x_1(t)\right] \tag{11}$$

where C is the consumer operator of AEO.

If a consumer $x_i(t)$ is a carnivorous animal, it can prey on other consumers with higher energy levels, as:

$$x_i(t+1) = x_i(t) + C\left[x_i(t) - x_j(t)\right] \tag{12}$$

where $i = 2,3,\cdots,n$; j is a random integer in $[2,\ i-1]$.

If a consumer $x_i(t)$ is selected as an omnivore, it updates its position based on the position of the producer and other consumers with higher energy levels, gives

$$\begin{aligned} x_i(t+1) = x_i(t) + C\{&r_2\left[x_i(t) - x_1(t)\right] + \\ &(1-r_2)\left[x_i(t) - x_j(t)\right]\} \end{aligned} \tag{13}$$

where r_2 is a random number uniformly distributed within $[0,\ 1]$.

The AEO decomposition operator mechanism makes each individual $x_i(t)$ in the population scatter around the current best solution (decomposer), as follows:

$$x_i(t+1) = x_n(t) + D\left[\varepsilon x_n(t) - h x_i(t)\right] \tag{14}$$

$$D = 3\boldsymbol{u} \tag{15}$$

$$\varepsilon = r_3 \cdot \mathrm{randi}([1, 2]) - 1 \tag{16}$$

$$h = 2r_3 - 1 \tag{17}$$

where D is the decentralized factor; $\boldsymbol{u}$ is a random vector or random number subject to standard normal distribution; r_3 is a random number uniformly distributed within $[0,\ 1]$; and randi([1, 2]) is used for randomization produces a positive integer 1 or 2.

B. Primal MRFO

There are three foraging strategies in MRFO, i.e., chain foraging, cyclone foraging, and somersault foraging [37].

In chain foraging, food source $x_{\mathrm{best}}(t)$ represents the location of the current optimal solution. Besides, each individual $x_i(t)$ updates its position towards the previous generation of individual $x_{i-1}(t)$ and the food source position during the iteration, forming a chain foraging operator, gives

$$x_i(t+1) = \begin{cases} x_i(t) + \boldsymbol{r}\left[x_{\mathrm{best}}(t) - x_i(t)\right] + \\ \qquad \alpha\left[x_{\mathrm{best}}(t) - x_i(t)\right], i = 1 \\ x_i(t) + \boldsymbol{r}\left[x_{i-1}(t) - x_i(t)\right] + \\ \qquad \alpha\left[x_{\mathrm{best}}(t) - x_i(t)\right], \\ i = 2,3,\cdots,n \end{cases} \tag{18}$$

where α is the weight coefficient.

Cyclone foraging strategy is considered in two parts, to enhance the global search capability of the MRFO in the pre-iterative stage, a random vector $\boldsymbol{x}_r$ is introduced to guide the individual $x_i(t)$ to update its position in the search space, which yields

$$x_i(t+1) = \begin{cases} \boldsymbol{x}_r + \boldsymbol{r}\left[\boldsymbol{x}_r - x_i(t)\right] + \\ \qquad \beta\left[\boldsymbol{x}_r - x_i(t)\right], i = 1 \\ \boldsymbol{x}_r + \boldsymbol{r}\left[x_{i-1}(t) - x_i(t)\right] + \\ \qquad \beta\left[\boldsymbol{x}_r - x_i(t)\right], i = 2,3,\cdots,n \end{cases} \tag{19}$$

$$\beta = 2\exp\left(\boldsymbol{r}_4 \frac{t_{\max} - t + 1}{t_{\max}}\right)\sin(2\pi \boldsymbol{r}_4) \tag{20}$$

where $\boldsymbol{r}_4$ is a random vector that follows a uniform distribution in $[0,1]$.

In the late iteration of the MRFO, food source $x_{\mathrm{best}}(t)$ is considered as a reference, and each approaches the food source in a spiral motion, as follows:

$$x_i(t+1) = \begin{cases} x_{\mathrm{best}}(t) + \boldsymbol{r}\left[x_{\mathrm{best}}(t) - x_i(t)\right] + \\ \qquad \beta\left[x_{\mathrm{best}}(t) - x_i(t)\right], i = 1 \\ x_{\mathrm{best}}(t) + \boldsymbol{r}\left[x_{i-1}(t) - x_i(t)\right] + \\ \qquad \beta\left[x_{\mathrm{best}}(t) - x_i(t)\right], \\ i = 2,3,\cdots,n \end{cases} \tag{21}$$

The third foraging strategy of MRFO is somersault foraging, the mathematical model can be described as:

$$x_i(t+1)=x_i(t)+S\left[\boldsymbol{r}_2 x_{\text{best}}(t)-\boldsymbol{r}_3 x_i(t)\right] \tag{22}$$

where S is the somersault factor.

C. Design of EMCO

Firstly, the decomposition operator mechanism of AEO is introduced into EMCO, it makes each individual gradually stay away from the producer with the worst fitness in the iteration. In addition, the chain and cyclone foraging strategies of MRFO can attract (especially in the later stage of the iteration) each individual to approach the food source with the best fitness. These two operations have similar features, thus EMCO retains the chain and cyclone foraging strategies of MRFO. Moreover, to prevent the algorithm from blindly searching, EMCO simplifies the cyclone foraging strategy of MRFO. Equation (18) and (21) can be further simplified as

$$\begin{aligned} x_i(t+1)=x_i(t)+\boldsymbol{r}\left[x_{i-1}(t)-x_i(t)\right]+\\ \alpha\left[x_{\text{best}}(t)-x_i(t)\right] \end{aligned} \tag{23}$$

$$\begin{aligned} x_i(t+1)=x_{\text{best}}(t)+\boldsymbol{r}\left[x_{i-1}(t)-x_i(t)\right]+\\ \beta\left[x_{\text{best}}(t)-x_i(t)\right] \end{aligned} \tag{24}$$

At last, the somersault factor in (22) is modified from $S=2$ to $S=3\boldsymbol{\xi}$, which can overcome the defect of insufficient global search ability caused by the aforementioned improvements. And $\boldsymbol{\xi}$ is a random vector or random number subject to the standard normal distribution, the optimization framework of EMCO is shown in Fig. 2.

IV. Optimal Array Layout Design of WEC Based on EMCO

A. Fitness Function

To further reveal and utilize the constructive interactions among HWWECs, optimization of HWWECs array is applied to find the optimal position of HWWECs and to maximize absorbed power of HWWECs array, that is, the value of q-factor should be maximized. Hence, the fitness function is chosen as:

$$\begin{aligned} q_{\text{best}}&=\max(q_1,q_2,\ldots,q_t),1\leqslant t\leqslant t_{\max}\\ q&=\frac{P_\Sigma}{NP_0} \end{aligned} \tag{25}$$

B. Constraints

Considering the construction and installation of HWWEC in reality, the distance between each HWWEC must keep above 50 m. Therefore, the coordinates of HWWECs should satisfy the following constraints:

$$\begin{cases} x_{io}\in(0,U_{\text{Lmax}}),\ i=1,2,\cdots,N\\ y_{io}\in(0,U_{\text{Wmax}}),\ i=1,2,\cdots,N\\ d_{\text{save}}=\sqrt{(x_{io}-x_{jo})^2+(y_{io}-y_{jo})^2}\geqslant 50,\\ i,j=1,2,\cdots,N,\ i\neq j \end{cases} \tag{26}$$

where x_{io} and y_{io} represent the coordinate of the ith HWWEC; U_{Lmax} and U_{Wmax} are the maximum length and width of the sea areal; and d_{save} is the safe distance between each HWWEC.

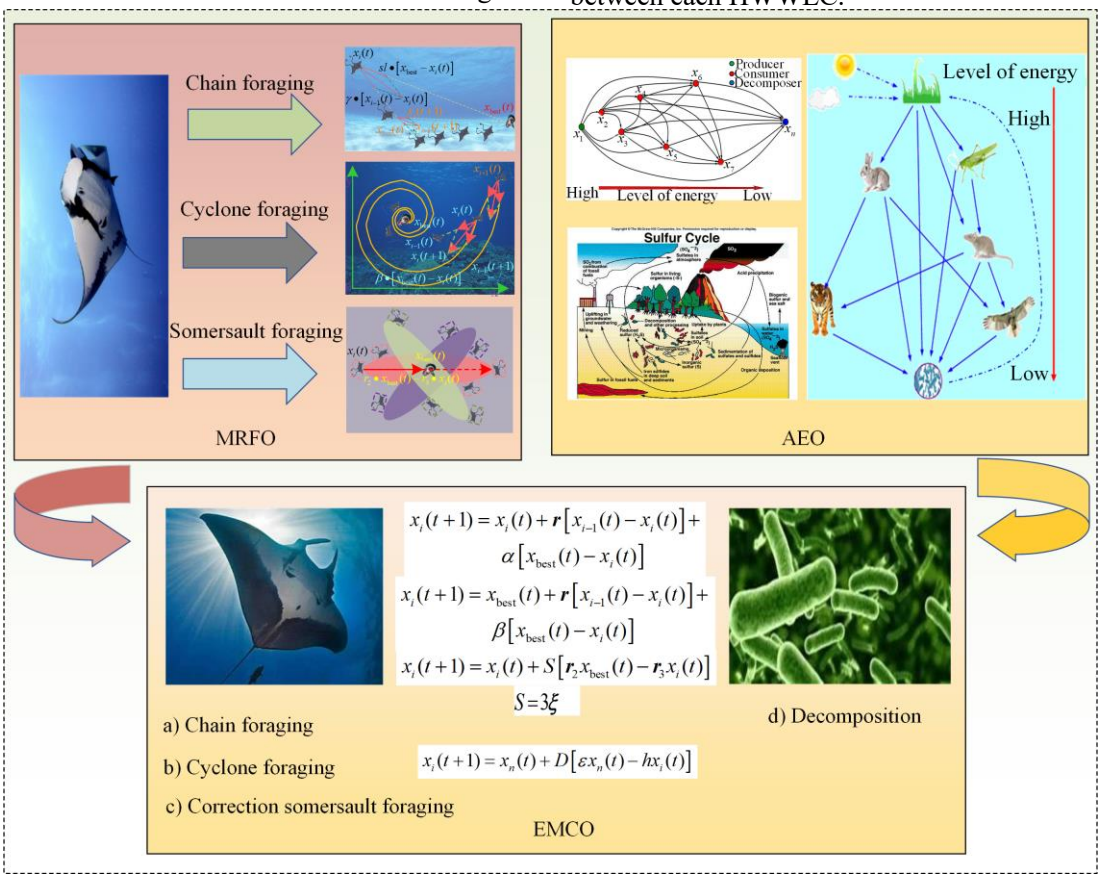

Fig. 2. Optimization framework of EMCO.

C. Execution Process

Firstly, the initial population is generated by EMCO, which is the initial array of HWWEC. Then, optimization iterations are carried out based on the mechanism of EMCO. Finally, the optimal layout of the HWWEC array can be realized. To ensure the diversity of the initial population and enhance its coverage of the search space, each individual is randomly initialized by (9). Furthermore, EMCO follows the bounds-checking rules of AEO and MRFO, and individuals that exceed the boundary can be reinitialized. All in all, the detailed execution process of EMCO and the flow chart of EMCO to optimize the layout of HWWECs array are described in Table I and Fig. 3, respectively. Note that rand is a random number uniformly distributed within $[0,1]$.

TABLE I
THE DETAILED EXECUTION PROCESS OF EMCO

INPUT: n (number of population), $t_{\max}$ (maximum number of iterations), N (number of HWWECs);
Initialize the positions of individuals by (9) and (26);
Calculate the fitness of each individual by (6) and (7); save the best fitness q_{best} and corresponding position x_{best};
WHILE $t \leqslant t_{\max}$
  FOR1 i =1~n
    IF1 rand<0.5
      Update the position of individual x_i using (23);
    EISE IF1
      Update the position of individual x_i using (24);
    END IF1
    Correct the position of each individual based on (26);
    Calculate the fitness of each individual by (6) and (7);
    Save the best fitness $q_{\text{best}}(t)$ and corresponding position $x_{\text{best}}(t)$;
  END FOR1
  FOR2 i =1~n
    IF2 $t/t_{\max}$<rand
      Update the position of individual x_i using (22), $S = 3\xi$;
    EISE IF2
      Update the position of individual x_i using (14);
    END IF2
    Correct the position of each individual based on (26);
    Calculate the fitness of each individual by (6) and (7);
    Save the best fitness $q_{\text{best}}(t)$ and corresponding position $x_{\text{best}}(t)$;
  END FOR2
END WHILE
OUTPUT: Best solution x_{best} and the best fitness q_{best}.

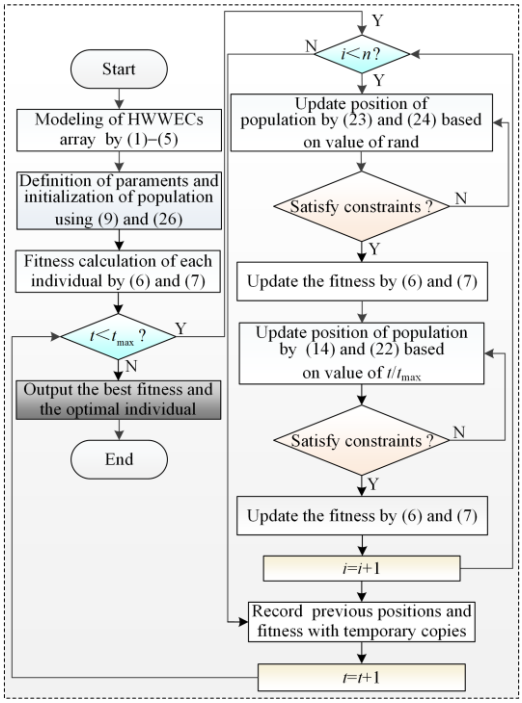

Fig. 3. Flowchart of EMCO-based layout optimization of HWWECs array.

V. CASE STUDIES

In this section, the optimization results of the experiments for developing the performance of HWWECs arrays are presented. Besides, wind-wave conditions are set to wind speed = 14 m/s, wave height = 1.9 m, and wave frequency = 0.7 rad/s. Moreover, the direction of wind-wave propagation is from left to right. The wind speed is above the rated wind speed for Vestas V27–225 kW WT. All in all, the main parameters of HWWEC system are tabulated in Table II.

EMCO is applied to implement four different scales HWWECs arrays optimization, i.e., 3-HWWEC, 5-HWWEC, 8-HWWEC, and 20-HWWEC. Meanwhile, the array optimization performance of five MhAs, including AEO [36], MRFO [37], GWO [45], CGO [46], and HBA [47] are compared with that of EMCO. The main parameters of various MhAs are shown in Table III.

To fairly evaluate and compare the performance of various algorithms in terms of convergence speed, scalability, and searchability, the population size n and the maximum iteration number $t_{\max}$ are uniformly set as $n = 60$ and $t_{\max} = 400$. Each algorithm is executed twenty times, and the best result among these twenty runs in terms of maximum output power andof WEC array is selected as the performance metric for evaluating the algorithm in array optimization.

TABLE II
THE MAIN PARAMETERS OF HWWEC AND WIND-WAVE CONDITIONS

Parameters	Value
FWT Rotor diameter D_{FWT} (m)	27
Cut-in wind speed $V_{\mathrm{cut\_in}}$ (m/s)	3.5
Rated wind speed V_{rated} (m/s)	11
Cut-out wind speed $V_{\mathrm{cut\_out}}$ (m/s)	22.5
Air density ρ_a (kg/m^3)	1.29
WEC buoy diameter D_{WEC} (m)	10
Submergence depth H_{sub} (m)	6
PTO spring coefficient K_{pto} (kN/m)	387
PTO damping coefficient B_{pto} (kN/m)	161
Ocean depth H_{ocean} (m)	50
Water density ρ_β (kg/m^3)	1020
Gravitational acceleration g (m/s^2)	9.81
Wave height H_{wave} (m)	1.9
Wave-wind propagation angle θ (rad)	0

TABLE III
THE MAIN PARAMETERS OF VARIOUS METHODS

Algorithms	Parameters	Value
EMCO	D (Decentralized factor)	$D=3u,\ u\sim N(0,\ 1)$
	S (Somersault factor)	$S=3\xi,\ \xi\sim N(0,\ 1)$
AEO	D (Decentralized factor)	$D=3u,\ u\sim N(0,\ 1)$
MRFO	S (Somersault factor)	2
GWO	$\vec{a}$ (Convergence factor)	a number which linearly decreases from 2 to 0 during the iteration process
CGO	a_i (Movement limitation factor)	a random number which is distributed uniformly in the range of $[0,\ 1]$
HBA	C (Constant)	2
	β (Predation ability)	6

Note that $\boldsymbol{u}\sim N(0,\ 1)$ represent $\boldsymbol{u}$ is a random vector or random number subject to standard normal distribution.

Moreover, each method is executed independently for 20 iterations to gather statistical insights, with the optimal outcome from each approach being documented and contrasted. To clearly describe the interaction between HWWECs and meet the constraint conditions, the sea areas of the four case studies are 300 m × 300 m, 500 m × 500 m, 1000 m × 1000 m, and 1000 m × 1000 m, respectively. Lastly, all computational resources are set at the same level and executed on Matlab R2022b platform by a personal computer with Intel (R) Core (TM) i5 CPU at 2.9 GHz and 32 GB of RAM.

A. Scenario 1: 3-HWWEC Array

Here, the power of a single isolated HWWEC to absorb wind and wave energy is calculated under the wind-wave conditions specified in this paper, which is 779 700 W. The convergence curves of q-factor for 3-HWWEC array obtained by various algorithms are shown in Fig. 4(a). It is easy to observe that q-factor of layouts optimized by various algorithms are more than 1. And all algorithms can find the globally optimal solution (q-factor = 1.0476) with different convergence rates except CGO. Especially EMCO, HBA, and MRFO have great performance in convergence rate, they converge at the 53rd, 70th, and 138th times respectively. Furthermore, total absorbed power P_Σ of HWWECs array based on 20 independent runs is presented in Fig. 4(b), which clearly describes the distribution and upper/lower bounds of absorbed power for each method. Apparently, EMCO harvests satisfactory performance on stability compared with other algorithms, although the maximum fitness value of MRFO is better than that of EMCO. In contrast, CGO performs poorly in terms of search capability compared with other algorithms.

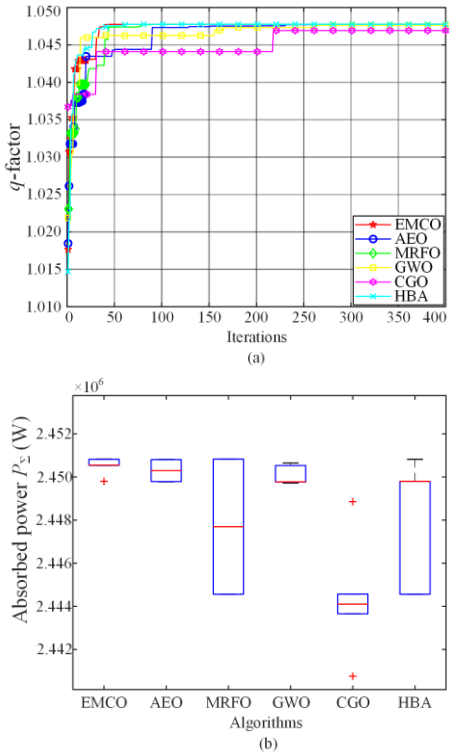

Fig. 4. Results of 3-HWWEC array obtained by various algorithms. (a) Convergence curves of q-factor . (b) Box-and-whiskers chart.

Additionally, Table IV summarizes the best results of six methods based on 20 independent runs of each method. One can easily see that the total absorbed powers are basically around 2450.8 kW in five methods i.e., EMCO, MRFO, AEO, GWO, and HBA. Besides, there is a difference in the optimal layout obtained by the mentioned five methods. However, the total absorbed power difference of each method is only within 0.015 kW. Therefore, this low-dimensional simulation experiment verifies that HWWECs array optimization has multiple optimal solutions.

At last, based on each HWWEC's absorbed power P_j and corresponding coordinates from Table IV, six 3-HWWEC layouts optimized by various algorithms are exhibited in Fig. 5. It is not surprising that the HWWEC face the incoming waves have the highest absorbed power in the left of HWWECs farm, which shows the fidelity of optimization results in this work.

TABLE IV
BEST EXPERIMENTAL RESULTS OF 3-HWWEC LAYOUT OPTIMIZED BY VARIOUS ALGORITHMS

Algorithms	HWWEC number j	Abscissa X (m)	Ordinate Y (m)	P_j (W)	P_Σ (W)	q-factor
EMCO	1	53	25	838 662.74	2 450 818.90	1.0478
	2	174	177	785 308.26		
	3	116	296	826 847.90		
AEO	1	160	19	826 936.74	2 450 815.32	1.0478
	2	98	290	838 565.89		
	3	218	139	785 312.69		
MRFO	1	47	288	838 681.52	2 450 827.89	1.0478
	2	167	137	785 326.58		
	3	109	17	826 819.78		
GWO	1	118	122	857 242.82	2 450 530.24	1.0476
	2	298	300	784 744.56		
	3	178	0	808 542.86		
CGO	1	64	31	802 537.72	2 448 852.78	1.0469
	2	122	300	789 828.12		
	3	3	150	856 486.94		
HBA	1	299	153	785 307.45	2 450 827.61	1.0477
	2	241	273	826 809.14		
	3	179	2	838 711.02		

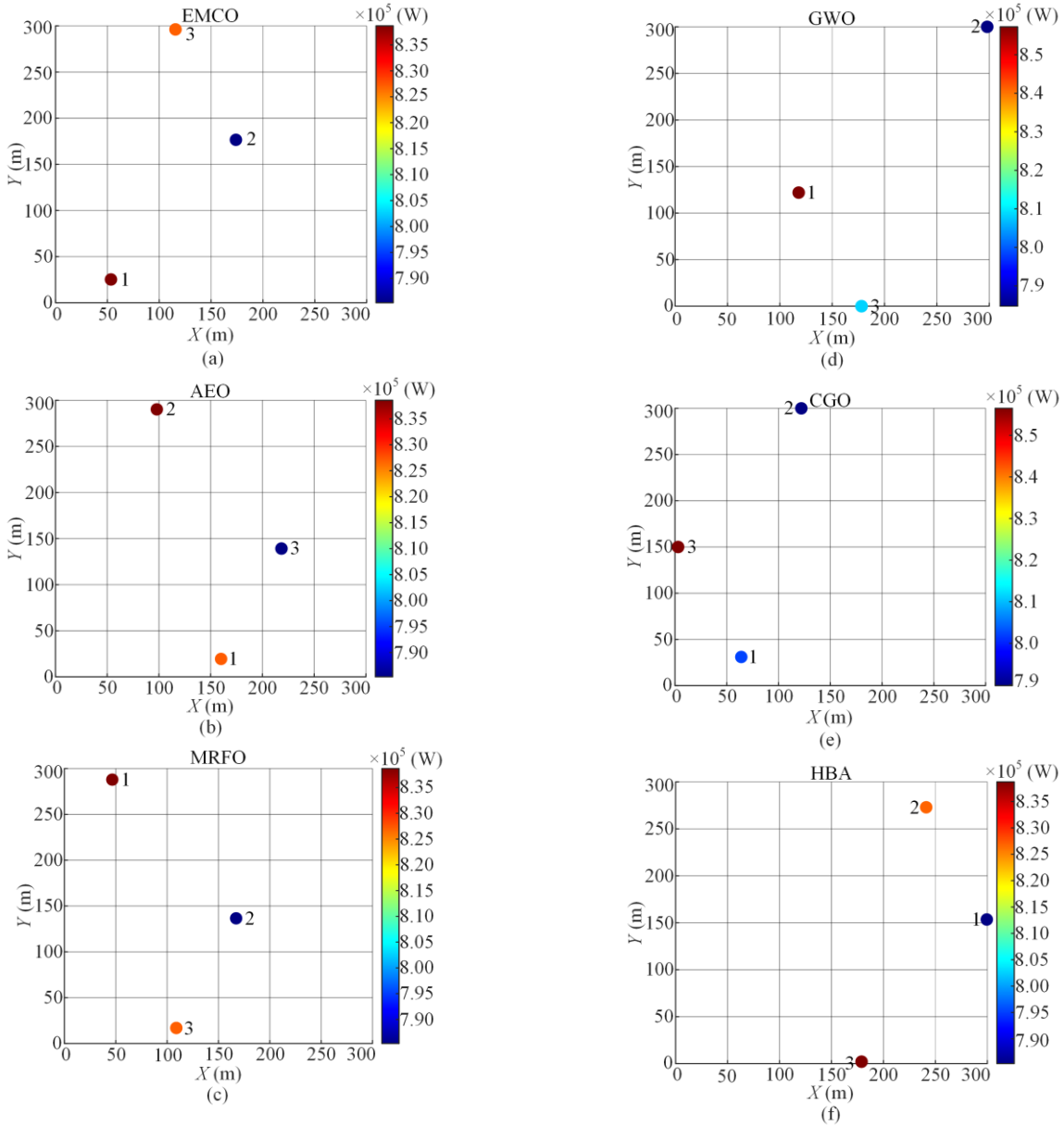

Fig. 5. Best-found 3-HWWEC layouts obtained by various methods. (a) EMCO. (b) AEO. (c) MRFO. (d) GWO. (e)CGO. (f) HBA.

B. Scenario 2: 5-HWWEC Array

In this case, the optimized performance of six algorithms for HWWECs array will be further compared by changing the number of HWWECs and sea area in Scenario 1. The convergence curves of q-factor for 5-HWWEC array obtained by various algorithms are shown in Fig. 6(a). It is easy to see that HBA and CGO have fast convergent speeds. However, EMCO can acquire the maximum q-factor in six methods, which effectively verifies the best global search capacity of EMCO. Besides, Fig. 6(b) depicts the box-and-whiskers chart for optimal layout obtained by six methods. One can easily see that EMCO capable to obtain a well-arranged 5-HWWEC layout with huge absorbed power. Meanwhile, the performance of CGO on stability is higher than that of EMCO, but its fitness value is the smallest among all algorithms. Therefore, in the 5-HWWEC array optimization experiment, different algorithms show their advantages in terms of convergence rate and searchability.

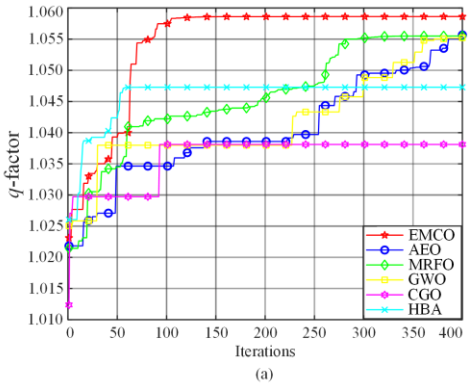

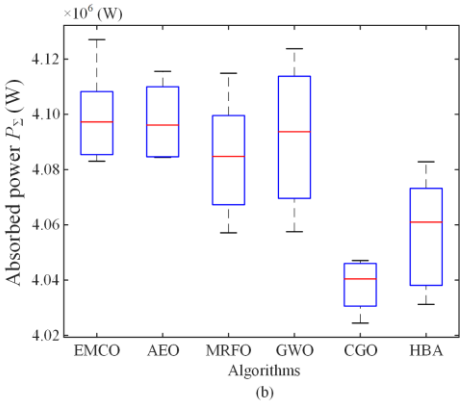

Fig. 6. Results of 5-HWWEC array obtained by various algorithms. (a) Convergence curves of q-factor. (b) Box-and-whiskers chart.

Furthermore, Table V summarizes the best results and each HWWEC's absorbed power in the array obtained by various methods. One can easily observe that the value of q-factor for EMCO is close to 1.059, which validates that EMCO can effectively explore the constructive interaction between floats in the HWWECs array. Meanwhile, it can generate the highest absorbed power of 4 127 052.23 W in all algorithms. In particular, q-factor obtained by EMCO can be improved by 0.28%, 0.30%, 0.32%, 1.96%, and 1.08% compared with that of AEO, MRFO, GWO, CGO, and HBA, respectively.

At last, based on the statistical results of Table V, six 5-HWWEC array layouts are exhibited in Fig. 7. It can be clearly seen that EMCO is able to modify the placement of each HWWEC successfully, which improves the total absorbed power of HWWECs array significantly.

TABLE V
BEST EXPERIMENTAL RESULTS OF 5-HWWEC LAYOUT OPTIMIZED BY VARIOUS ALGORITHMS

Algorithms	HWWEC number j	Abscissa X (m)	Ordinate Y (m)	P_j (W)	P_Σ (W)	q-factor
EMCO	1	154	152	890 182.68	4 127 052.24	1.0586
	2	399	364	790 360.70		
	3	337	491	825 232.83		
	4	212	20	812 809.09		
	5	93	291	808 466.93		
AEO	1	320	252	833 587.23	4 115 543.44	1.0557
	2	319	148	826 834.34		
	3	320	359	828 746.81		
	4	320	457	815 047.12		
	5	315	50	811 327.94		
MRFO	1	286	346	788 484.46	4 114 879.99	1.0555
	2	226	207	842 852.38		
	3	228	99	827 070.47		
	4	226	0	811 964.81		
	5	164	494	844 507.88		
GWO	1	271	500	843 563.22	4 113 782.69	1.0552
	2	335	108	827 867.27		
	3	333	216	843 804.42		
	4	333	10	811 274.33		
	5	392	355	787 273.45		
CGO	1	345	63	789 026.23	4 047 088.62	1.0381
	2	236	383	795 564.15		
	3	220	491	821 987.33		
	4	176	235	853 786.65		
	5	109	67	786 724.26		
HBA	1	0	0	805 932.39	4 082 829.74	1.0473
	2	500	422	804 322.46		
	3	0	187	845 256.97		
	4	0	97	822 046.91		
	5	500	500	805 271.01		

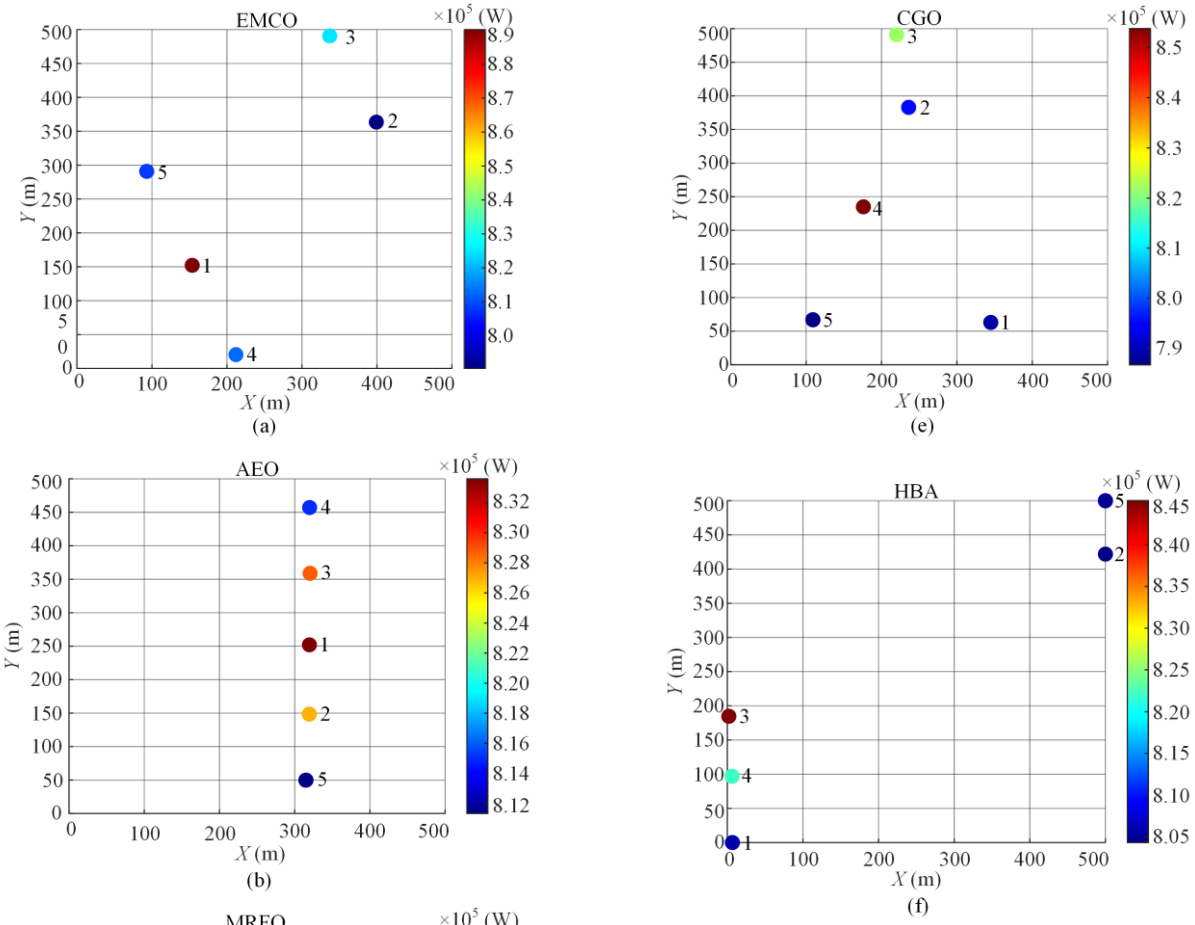

Fig. 7. Best-found 5-HWWEC layouts obtained by various methods. (a) EMCO. (b) AEO. (c) MRFO. (d) GWO. (e) CGO. (f) HBA.

C. Scenario 3: 8-HWWEC Array

Compared to the optimization for 3-HWWEC and 5-HWWEC layouts, the calculated cost for the 8-HWWEC layout is more expensive, while the complexity of searching space is much higher due to hydrodynamic interactions among floats. According to the investigations of convergence rate for six algorithms on optimization 8-HWWEC layout. One can find from Fig. 8(a) that EMCO and MRFO can obtain a large fitness value with fast convergence rates. However, q-factor of MRFO is lower than that of EMCO considerably, which fully demonstrates the strong ability of EMCO to explore and exploit array optimization, as well as to avoid being trapped into a local optimum. On the contrary, AEO, GWO, and HBA have not reached convergence throughout the entire iteration process, while CGO falls into local optima.

Furthermore, Fig. 8(b) depicts the box-and-whiskers chart for optimal layout obtained by six methods, which depends on the results of 20 independent runs of each algorithm. Obviously, EMCO achieves excellent performance on maximum absorbed power although AEO and CGO have well performance on stability.

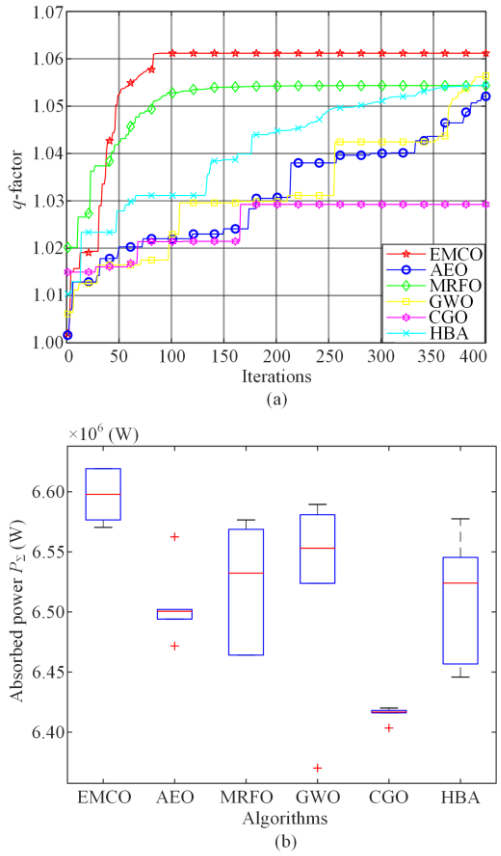

Fig. 8. Results of 8-HWWEC array obtained by various algorithms. (a) Convergence curves of q-factor. (b) Box-and-whiskers chart.

In addition, for further comparison of all applied methods, Table VI summarizes the best results of six methods. One can easily observe that the value of q-factor can be more than 1.05 optimized by EMCO, AEO, MRFO, GWO and CGO, especially the q-factor of array optimized by EMCO can be significantly increased to 1.061, which is the largest value in all q-factor. In the same way, based on the best position of 8-HWWEC and each HWWEC's absorbed power from Table VI, six 8-HWWEC layouts optimized are exhibited in Fig. 9. One can clearly observe that the HWWECs arrays optimized by EMCO, AEO, and MRFO all have eight HWWEC's absorbed power greater than 779 700 W, which proves that HWWEC can absorb more energy when arranged in the form of an array.

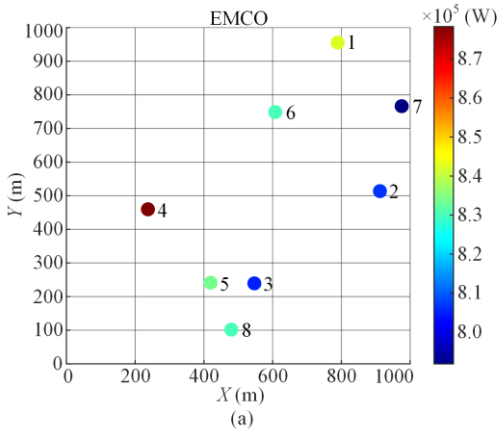

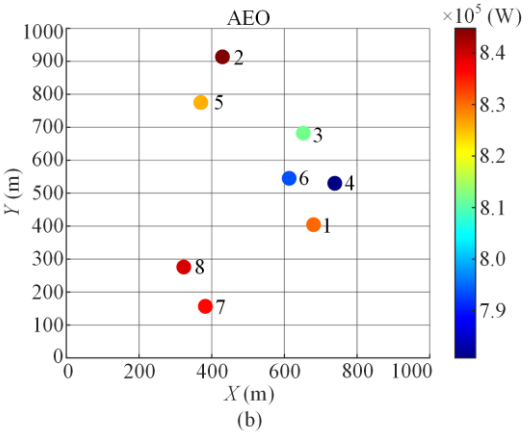

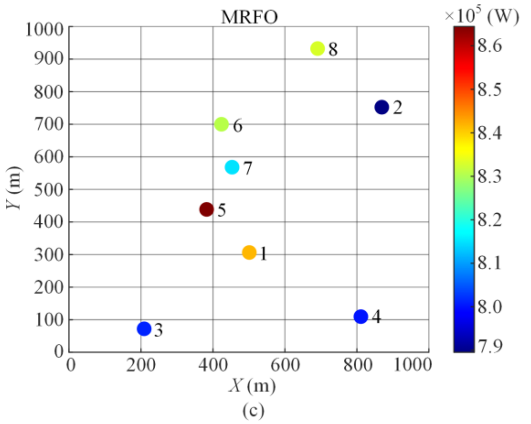

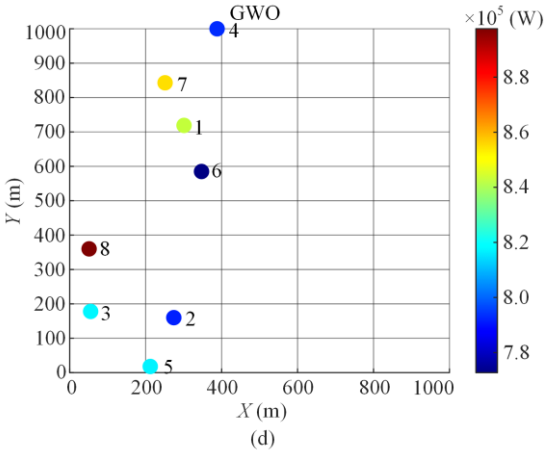

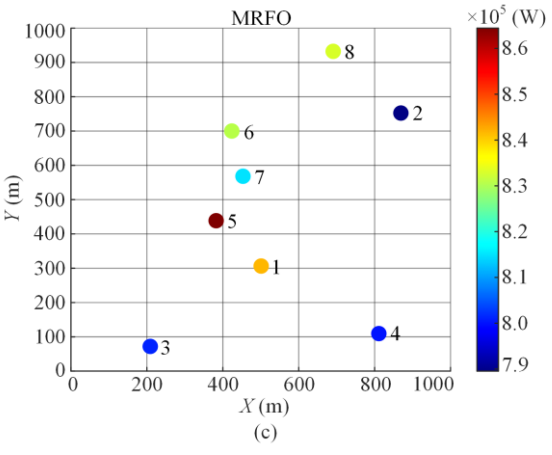

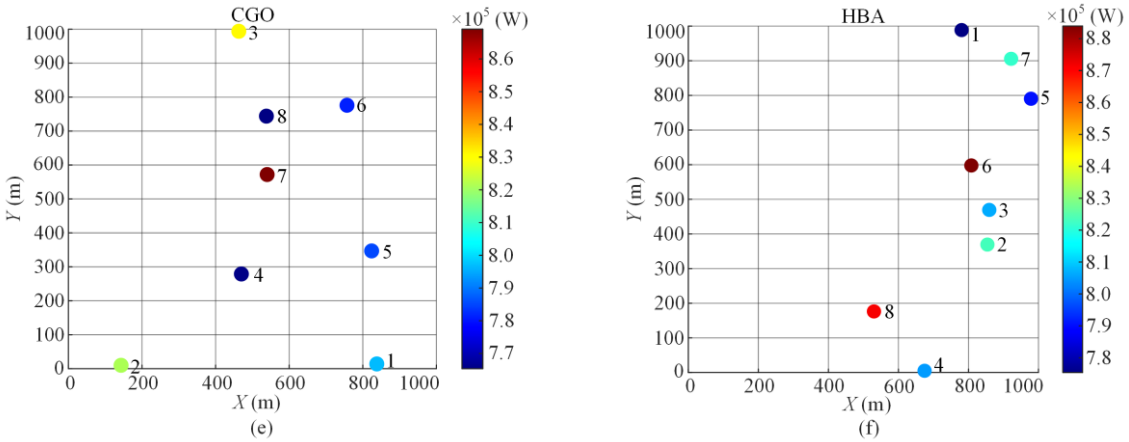

Fig. 9. Best-found 8-HWWEC layouts obtained by various methods.
(a) EMCO. (b) AEO. (c) MRFO. (d) GWO. (e) CGO. (f) HBA.

TABLE VI
BEST EXPERIMENTAL RESULTS OF 8-HWWEC LAYOUT OPTIMIZED BY VARIOUS ALGORITHMS

Algorithms	HWWEC number j	Abscissa X (m)	Ordinate Y (m)	P_j (W)	P_Σ (W)	q-factor
EMCO	1	789	955	842 508.55	6 619 237.66	1.0612
	2	912	514	806 944.94		
	3	547	239	805 364.07		
	4	237	460	878 292.80		
	5	419	241	833 908.37		
	6	607	749	830 292.83		
	7	975	766	791 859.47		
	8	480	102	830 066.64		
AEO	1	680	404	830 121.80	6 562 469. 51	1.0521
	2	430	914	844 752.89		
	3	652	682	812 036.73		
	4	739	530	780 837.22		
	5	370	775	825 582.64		
	6	613	545	793 819.76		
	7	382	157	836 243.59		
	8	323	276	839 074.88		
MRFO	1	501	306	841 507.20	6 576 582.90	1.0543
	2	869	752	789 538.25		
	3	209	72	801 352.17		
	4	811	110	800 230.04		
	5	382	439	864 429.44		
	6	424	700	830 843.66		
	7	453	568	815 385.27		
	8	691	932	833 296.88		
GWO	1	301	719	843 361.06	6 589 495.15	1.0564
	2	274	160	791 872.41		
	3	55	178	818 434.93		
	4	388	1000	793 286.91		
	5	212	18	817 785.07		
	6	347	585	772 713.28		
	7	251	843	854 496.73		
	8	51	360	897 544.75		
CGO	1	838	14	797 190.62	6 420 003.40	1.0292
	2	143	10	821 550.74		
	3	463	994	830 240.21		
	4	470	279	766 102.49		
	5	824	347	785 369.15		
	6	757	776	781 185.28		
	7	540	572	869 076.12		
	8	538	744	765 364.16		
HBA	1	780	989	775 384.91	6 577 511.00	1.0545
	2	854	369	822 939.11		
	3	859	469	807 094.69		
	4	675	5	805 179.70		
	5	979	790	790 280.80		
	6	808	598	883 922.53		
	7	922	906	821 596.42		
	8	530	176	871 112.85		

D. Scenario 4: 20-HWWEC Array

From the optimization results of the six algorithms in the previous three case studies, it can be found that EMCO and MRFO exhibit great performance in terms of maximum absorbed power and convergence speed, and CGO has the best performance in terms of stability during the search process. In the optimization layout of 20-HWWEC array, the convergence curves of q-factor obtained by various algorithms are shown in Fig. 10(a). It is easy to observe that q-factor of each array decreases significantly to less than 1, the destructive interaction between floats also increases with the growing number of HWWECs. Moreover, both GWO and CGO fall into local optima during the optimization process with the low value of q-factor . Meanwhile, four q-factor iteration curves obtained by EMCO, AEO, MRFO, and HBA have not reached a convergence state in the high-dimensional optimization experiment. Fortunately, EMCO can still outperform comparison methods in terms of the value of array q-factor , which fully demonstrates the strong ability of EMCO to explore and exploit array optimization.

Furthermore, absorbed power based on 20 independent runs is presented in Fig. 10(b). Obviously, EMCO achieves excellent performance on maximum absorbed power although its stability is weaker than that of CGO. Therefore, there are some limitations in convergence rate and stability for EMCO in high-dimension optimization experiments.

Meanwhile, Table VII provides the 20-HWWEC array optimization results of various methods, q-factor obtained by EMCO can be improved by 1.82%,1.25%, 3.37%, 3.62%, and 1.33% compared with that of AEO, MRFO, GWO, CGO, and HBA, respectively.

Lastly, according to the coordinates and absorbed power of each HWWEC displayed in Table VII, Fig. 11 depicts 20-HWWEC layouts obtained by various methods. Although the value of q-factor is less than 1, constructive interferences result in individual HWWECs having an absorbed power P_j greater than 779 700 W at certain locations, e.g., the HWWECs located at (456, 23), (966, 498) and (677, 46), etc.

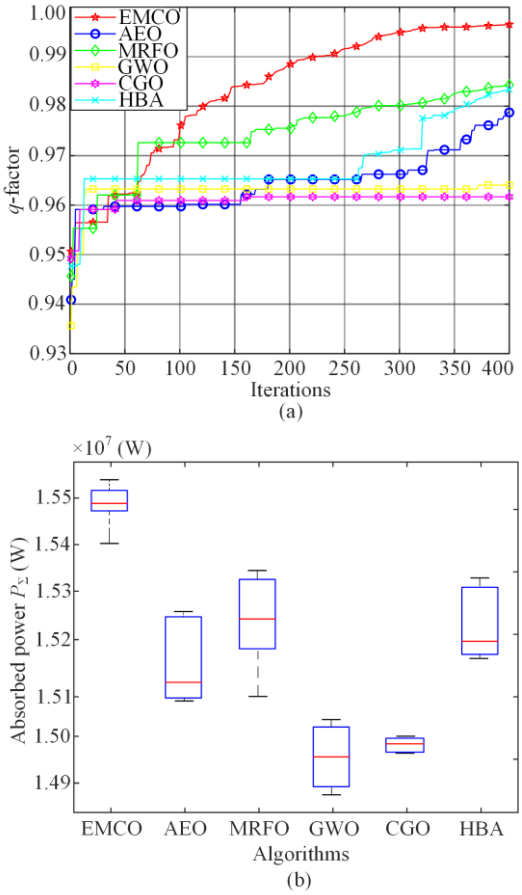

Fig. 10. Results of 20-HWWEC array obtained by various algorithms. (a) Convergence curves of q-factor. (b) Box-and-whiskers chart.

TABLE VII
BEST EXPERIMENTAL RESULTS OF 20-HWWEC LAYOUT OPTIMIZED BY VARIOUS ALGORITHMS

Algorithms	HWWEC number j	Abscissa X (m)	Ordinate Y (m)	P_j (W)	P_Σ (W)	q-factor
EMCO	1	518	196	845 674.99	15 539 668.32	0.9965
	2	521	432	712 192.78		
	3	237	695	654 131.75		
	4	129	1000	772 795.69		
	5	723	546	747 752.26		
	6	876	679	722 567.97		
	7	495	529	732 596.29		
	8	456	23	825 121.03		
	9	123	260	746 405.97		
	10	0	42	766 484.02		
	11	966	498	807 410.39		
	12	634	725	777 379.93		
	13	975	295	793 054.68		
	14	636	926	875 081.47		
	15	946	694	781 347.17		
	16	677	46	838 141.82		
	17	520	278	757 499.60		
	18	429	948	825 867.93		
	19	527	374	783 123.04		
	20	530	759	775 039.55		
AEO	1	280	68	744 778.55	15 262 287.27	0.9787
	2	904	606	801 936.82		
	3	661	556	794 241.42		
	4	850	323	796 093.28		

Continued

Algorithms	HWWEC number j	Abscissa X (m)	Ordinate Y (m)	P_j (W)	P_Σ (W)	q-factor
	5	258	294	794 068.23		
	6	556	597	747 468.37		
	7	648	108	747 142.33		
	8	228	449	707 813.47		
	9	872	94	796 284.20		
	10	282	989	773 611.42		
	11	825	768	751 733.47		
	12	73	795	711 000.19		
	13	657	946	781 909.46		
	14	67	93	722 535.45		
	15	879	24	812 963.17		
	16	56	449	749 284.92		
	17	122	247	719 592.50		
	18	670	770	728 196.81		
	19	675	456	796 395.14		
	20	986	870	785 238.07		
MRFO	1	647	1000	720 499.39	15 348 405.97	0.9842
	2	423	494	847 857.63		
	3	0	1000	714 942.47		
	4	109	718	809 755.12		
	5	726	757	837 346.88		
	6	338	722	818 289.88		
	7	0	0	683 348.56		
	8	1000	1000	774 885.77		
	9	0	426	810 483.88		
	10	88	0	717 819.15		
	11	149	0	746 396.31		
	12	615	61	791 478.09		
	13	813	373	826 643.70		
	14	748	1000	741 598.69		
	15	1000	0	778 405.38		
	16	160	264	694 635.79		
	17	474	1000	727 995.16		
	18	763	244	823 770.44		
	19	446	283	741 099.34		
	20	368	1000	741 154.36		
GWO	1	442	142	733 939.615	15 033 525.63	0.9640
	2	411	768	820 496.900 1		
	3	683	288	729 231.925 1		
	4	427	40	864 371.575 3		
	5	813	274	793 883.274 8		
	6	855	495	776 270.872 7		
	7	818	823	763 119.584 2		
	8	526	934	711 038.037 7		
	9	326	4	775 792.705 6		
	10	363	532	702 393.025 9		
	11	324	55	716 186.206 3		
	12	647	468	751 103.384 1		
	13	362	129	640 033.217 2		
	14	20	874	731 062.540 9		
	15	786	353	835 616.840 1		
	16	348	629	675 079.389 6		
	17	572	605	772 779.637 3		
	18	308	882	781 132.424		
	19	270	207	643 963.175 3		
	20	791	597	816 031.302 6		
CGO	1	463	781	739 043.70	14 996 614.18	0.9617
	2	129	677	644 122.06		
	3	278	426	825 461.69		
	4	510	32	865 905.07		
	5	116	758	820 119.13		
	6	761	695	800 696.80		
	7	372	277	621 767.33		
	8	618	999	789 901.16		
	9	295	558	759 693.49		
	10	901	489	781 838.58		
	11	177	147	721 244.21		
	12	639	225	828 494.85		
	13	334	949	778 597.56		
	14	139	63	766 461.49		

Continued

Algorithms	HWWEC number j	Abscissa X (m)	Ordinate Y (m)	P_j (W)	P_Σ (W)	q-factor
	15	405	103	722 152.32		
	16	70	323	654 004.55		
	17	694	359	742 317.45		
	18	131	272	672 118.98		
	19	823	851	776 535.04		
	20	266	273	686 550.19		
HBA	1	0	621	786 994.08	15 334 406.59	0.9834
	2	1000	632	811 441.46		
	3	594	715	672 650.37		
	4	446	309	741 186.76		
	5	1000	692	773 800.55		
	6	626	982	725 360.23		
	7	153	1000	811 441.93		
	8	63	234	730 771.30		
	9	0	0	719 971.57		
	10	773	308	762 764.84		
	11	1000	539	821 976.11		
	12	1000	443	801 969.01		
	13	702	730	758 247.95		
	14	74	0	787 465.47		
	15	1000	1000	800 004.01		
	16	802	49	791 762.61		
	17	439	0	807 920.37		
	18	793	248	822 544.67		
	19	781	1000	732 257.21		
	20	0	1000	673 876.08		

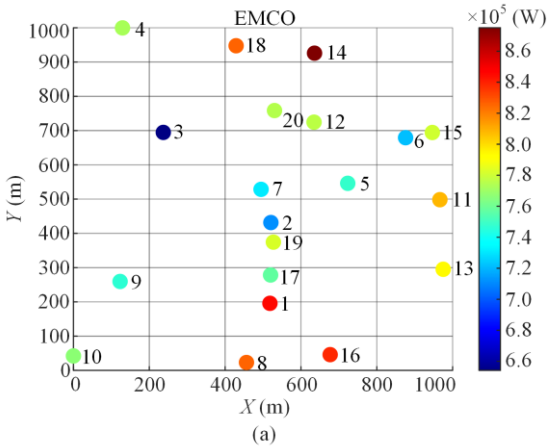

(a)

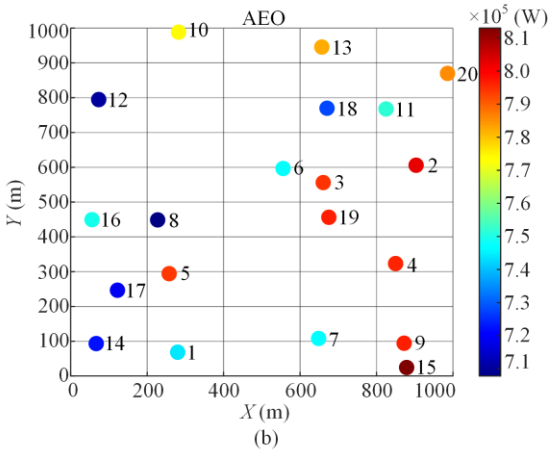

(b)

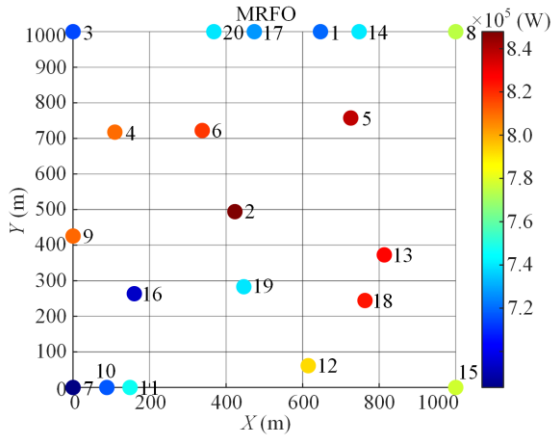

(c)

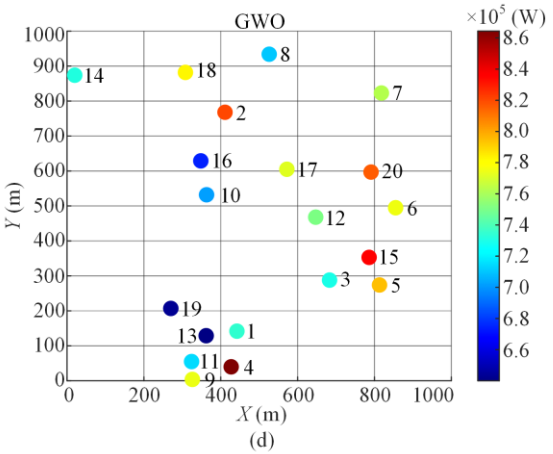

(d)

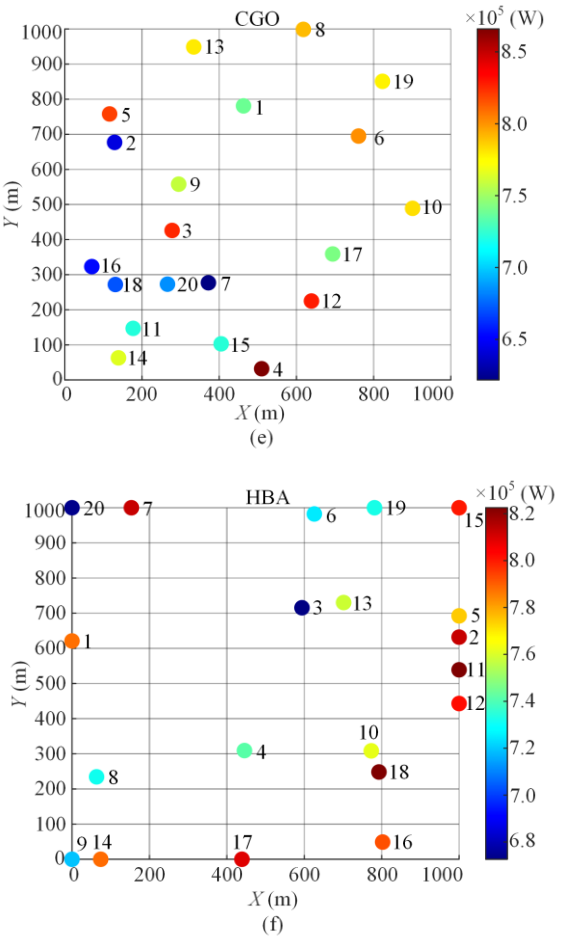

Fig. 11. Best-found 20-HWWEC layouts obtained by various methods. (a) EMCO. (b) AEO. (c) MRFO. (d) GWO. (e)CGO. (f) HBA.

VI. Conclusions

EMCO-based HWWECs array optimization is presented to explore the constructive interactions between HWWECs, upon which six points are drawn as follows:

1) A novel HWWEC is originally designed based on Vestas V27–225 kW WT and three-tether WEC. Compared with the traditional wave farm and offshore wind farm, far offshore co-located wind-wave energy farms can simultaneously capture offshore wind and wave energy, which dramatically improves energy utilization efficiency and saves space utilized and construction costs on the sea.

2) The global searching ability of EMCO is greatly improved through effectively integrating and modifying the original algorithms (AEO and MRFO) without introducing additional complex improvement mechanisms. As a result, the balance between local exploration and global search of EMCO is ensured.

3) EMCO and five typical competitive MhAs including AEO, MRFO, GWO, CGO, and HBA are simultaneously employed for layout optimization of four various HWWECs farms e.g., 3-HWWEC, 5-HWWEC, 8-HWWEC, and 20-HWWEC. The performances of algorithms are evaluated by total absorbed power P_{Σ} and q-factor of HWWECs farm.

4) In the small 3-HWWEC array scenario, simulation results effectively prove that there are multiple optimal solutions in the optimization of HWWECs array, and all methods can find them with different convergence rates except CGO. Besides, the array q-factor can be significantly increased to 1.0477.

5) The experimental results of 5-HWWEC and 8-HWWEC scenarios show that EMCO can achieve the best performances in the searching ability for optimal solutions. In particular, the maximum q-factor of 5-HWWEC array layout optimized via EMCO is increased by 0.28%, 0.30%, 0.32%, 1.96%, and 1.08% compared with that of AEO, MRFO, GWO, CGO, and HBA, individually. And q-factor of 8-HWWEC array obtained by EMCO can be improved by 0.87%, 0.65%, 0.45%, 3.10%, 0.04%, and 0.63% compared with that of AEO, MRFO, GWO, CGO, and HBA, respectively.

6) In the large 20-HWWEC scenario, q-factor of each array decreases slightly to less than 1. With the increase of the dimension, the complexity and calculation cost of optimization works becomes higher compared with 5-HWWEC and 8-HWWEC arrays. Thus, it is difficult for all algorithms to detect global optima in such a large HWWECs array. Fortunately, the total absorbed power obtained by EMCO can be enhanced by 1.82%, 1.25%, 3.37%, 3.62%, and 1.33% compared with that of AEO, MRFO, GWO, CGO, and HBA, respectively.

Future studies might focus on the following three aspects:

1) The technology of HWWEC system is still on its initial stage. The reason for this is that both WEC and FWT platforms have many subcategories. Meanwhile, it is tough to reach a common agreement about how to combine them together. Therefore, future research will combine different types of WEC and FWT to design suitable HWWEC systems for sea conditions in different geographical locations.

2) EMCO might be employed in larger-scale wave-wind farms in real-time to further evaluate its validity and feasibility.

3) Evaluation of the economy and safety of HWWECs array will be considered in the fitness function.

4) The habitats for marine life would be influenced by the construction of HWWECs array. Therefore, the impact of HWWECs array on the marine ecosystem will be studied in detail.

5) The model of HWWEC will be further improved, and the mutual effect of wake turbulence among offshore WTs will be further considered and studied. At the same time, research on the combination field of offshore photovoltaics and wave energy will also be explored.

ACKNOWLEDGMENT

Not applicable.

AUTHORS' CONTRIBUTIONS

Bo Yang: writing review and editing, writing original draft, and conceptualization. Jinhang Duan: writing original draft and data curation. Yunfeng Yan: writing review, editing and supervision. Bingqiang Liu: funding acquisition and formal analysis. Jianxiang Huang: visualization and data curation. Lin Jiang: supervision and resources. Rui Han: visualization and data curation. All authors read and approved the final manuscript.

FUNDING

This work is supported by the National Natural Science Foundation of China (No. 61963020 and No. 62263014) and Yunnan Provincial Basic Research Project (No. 202201AT070857).

AVAILABILITY OF DATA AND MATERIALS

Please contact the corresponding author for data material request.

DECLARATIONS

Competing interests: The authors declare that they have no known competing financial interests or personal relationships that could have appeared to influence the work reported in this paper.

AUTHORS' INFORMATION

Bo Yang received the Ph.D. degree in University of Liverpool, UK. (jointly sponsored by University of Liverpool and China Scholarship Council), in 2015. He is currently a professor with the School of Electrical Engineering, Kunming University of Science and Technology, Kunming, China. His research interests include intelligent optimization and control of renewable energy and energy storage system.

Jinhang Duan received her B.Eng. degree in Kunming University of Science and Technology, Kunming, China, in 2022. She is currently pursuing a M.Sc degree in degree in electronic engineering from Kunming University of Science and Technology, Kunming, China. Her research interests include the wave energy system array optimization.

Yunfeng Yan received the Ph.D. degree in Zhejiang University, Hangzhou, China, in 2019. She is currently working in the College of Electrical Engineering, Zhejiang University, Hangzhou, China. Her research interests include intelligent optimization and control of renewable energy and energy storage system.

Bingqiang Liu received his B.Eng. degree in Kunming University of Science and Technology, Kunming, China, in 2021. He is currently pursuing a M.Sc degree in degree in electronic engineering from Kunming University of Science and Technology, Kunming, China. His research interests include the wave energy system array optimization.

Jianxiang Huang received his B.Eng. degree in Central South University, Changsha, China. He is currently working in the Kunming Bureau of CSG EHV Transmission Company, Kunming, China. His research interests include renewable energy optimization and control.

Lin Jiang received the Ph.D. degree in University of Liverpool, UK, in 2001. He is currently a reader with the School of Department of Electrical Engineering and Electronics, University of Liverpool, UK. His research interests include intelligent optimization and control of renewable energy and energy storage system.

Rui Han currently working in the Electric Power Science Research Institute, State Grid Zhejiang Electric Power Company Ltd., Hangzhou, China. His research interests include renewable energy optimization and control.

REFERENCES

[1] Y. Chen, B. Yang, and Z. Guo *et al.*, "Dynamic reconfiguration for TEG systems under heterogeneous temperature distribution via adaptive coordinated seeker," *Protection and Control of Modern Power Systems*, vol. 7, no. 3, pp. 567-585, Jul. 2022.

[2] S. SHI, H. WU, and D. HUANG *et al.*,"Energy storage capacity configuration of an offshore wind farm considering the influence of complex ocean climate conditions," *Power System Protection and Control*, vol. 50, no. 10, pp. 172-179, May 2022. (in Chinese)

[3] B. Yang, Y. Li, and J. Li *et al.*, "Comprehensive summary of solid oxide fuel cell control: a state-of-the-art review," *Protection and Control of Modern Power Systems*, vol. 7, no. 3, pp. 523-553, Jul. 2022.

[4] B. Yang, H. Ye, and J. Wang *et al.*, "PV arrays reconfiguration for partial shading mitigation: recent advances, challenges and perspectives," *Energy Conversion and Management,* vol. 7, no. 3, pp. 1-31, May 2021.

[5] E. Loukogeorgaki, C. Michailides, and G. Lavidas *et al.*, "Layout optimization of heaving Wave Energy Converters linear arrays in front of a vertical wall," *Renewable Energy*, vol. 179, pp. 189-203, Mar. 2021.

[6] B. Yang, B. Liu, and H. Zhou *et al.*, "A critical survey of technologies of large offshore wind farm integration: Summary, advances, and perspectives," *Protection and Control of Modern Power Systems*, vol. 7, no. 2, pp. 233-264, Apr. 2022.

[7] I. Lopez, J. Andreu, and S. Ceballos *et al.*, "Review of wave energy technologies and the necessary power-equipment," *Renewable and Sustainable Energy Reviews*, vol. 27, pp. 413-434, May 2013.

[8] A. Copping, H. Battey, and J. Brown-Saracino *et al*., "An international assessment of the environmental effects of marine energy development," *Ocean and Coastal Management*, vol. 99, pp. 3-13, Apr. 2014.
[9] A. Saenz-Aguirre, J. Saenz, and A. Ulazia *et al*., "Optimal strategies of deployment of far offshore co-located wind-wave energy farms," *Energy Conversion and Management*, vol. 251, pp. 1-15, May 2021.
[10] M. D. Esteban, J. J. Diez, and J. S. Lopez *et al*., "Why offshore wind energy," *Renewable Energy,* vol. 36, no. 2, pp. 444-450, May 2010.
[11] S. Rasool, K. M. Muttaqi, and D. Sutanto *et al*., "Quantifying the reduction in power variability of co-located offshore wind-wave farms," *Renewable Energy*, vol. 185, pp. 1018-1033, Feb. 2022.
[12] J. Lyu, O. Abdelkhalik, and L. Gauchia, "Optimization of dimensions and layout of an array of wave energy converters," *Ocean Engineering*, vol. 195, no. 15, Nov. 2018.
[13] B. Yang, S. Wu, and H. Zhang *et al.*, "Wave energy converter array layout optimization: a critical and comprehensive overview," *Renewable and Sustainable Energy Reviews*, vol. 167, Oct. 2022.
[14] M. Melikoglu, "Current status and future of ocean energy sources: a global review," *Ocean Engineering*, vol. 148, pp. 563-573, Jan. 2018.
[15] S. Rasool, M. R. Islam, and K. M. Muttaqi *et al.*, "The grid connection of linear machine-based wave power generators," in *Advanced Linear Machines and Drive Systems (ALMDS)*, Singapore, Singapore, Sep. 2019, pp. 303-341.
[16] M. A. Mustapa, O. B. Yaakob, and Y. M. Ahmed *et al*., "Wave energy device and breakwater integration: a review," *Renewable and Sustainable Energy Reviews*, vol. 77, pp. 43-58, Sep. 2017.
[17] J. Hu, B. Zhou, and C. Vogel *et al*., "Optimal design and performance analysis of a hybrid system combing a floating wind platform and wave energy converters," *Applied Energy*, vol. 269, May 2020.
[18] S. Astariz, C. Perez-Collazo, and J. Abanades *et al*., "Co-located wind-wave farm synergies (operation & maintenance): a case study," *Energy Conversion and Management*, vol. 91, pp. 63-75, Feb. 2015.
[19] Z. Ti and X. Deng, "Layout optimization of offshore wind farm considering spatially inhomogeneous wave loads," *Applied Energy*, vol. 306, Jan. 2022.
[20] M. J. Muliawan, M. Karimirad, and T. Moan, "Dynamic response and power performance of a combined spar-type floating wind turbine and coaxial floating wave energy converter," *Renewable Energy*, vol. 50, no. 3, pp. 47-57, Feb. 2013.
[21] M. J. Muliawan, M. Karimirad, and Z. Gao *et al*., "Extreme responses of a combined spar-type floating wind turbine and floating wave energy converter (STC) system with survival modes," *Ocean Engineering*, vol. 65, no. 2, pp. 71-82, Jun. 2013.
[22] Y. Luan, C. Michailides, and Z. Gao *et al*., "Molding and analysis of a 5 MW semi-submersible wind turbine combined with three flap-type wave energy converters," in *ASME International Conference on Ocean*, San Francisco, USA, Jun. 2014, pp. 1-12.
[23] S. Astariz and G. Iglesias, "Selecting optimum locations for co-located wave and wind energy farms, part II: a case study," *Energy Conversion and Management*, vol. 122, pp. 599-608, Aug. 2016.
[24] J. S. Rony and D. Karmakar, "Coupled dynamic analysis of hybrid offshore wind turbine and wave energy converter," *Journal of Offshore Mechanics and Arctic Engineering*, vol.144, no. 3, pp. 1-13, Jun. 2022.
[25] N. Ren, Z. Ma, and T. Fan *et al*., "Experimental and numerical study of hydrodynamic responses of a new combined monopile wind turbine and a heave-type wave energy converter under typical operational conditions," *Ocean Engineering*, vol. 159, pp. 1-8, Jul. 2018.
[26] Y. Wang, W. Shi, and C. Michailides *et al*., "WEC shape effect on the motion response and power performance of a combined wind-wave energy converter," *Ocean Engineering*, vol. 250, Apr. 2022.
[27] B. Kaya and E. Oguz, "Investigation of layout optimization for offshore wind farms and a case study for a region in Turkey," *Ocean Engineering*, vol. 266, Dec. 2022.
[28] C. Harp and B. Dupont, "Wave energy converter array optimization: a genetic algorithm approach and minimum separation distance study," *Ocean Engineering*, vol. 162, pp. 148-156, Sep. 2018.
[29] A. Babarit, "On the park effect in arrays of oscillating wave energy converters," *Renewable Energy*, vol. 58, pp. 68-78, Oct. 2013.
[30] K. S. Eikrem, R. J. Lorentzen, and R. Faria *et al*., "Offshore wind farm layout optimization using ensemble methods," *Renewable Energy*, vol. 216, Nov. 2023.
[31] J. Wu, S. Shekh, and N. Y. Sergiienko *et al*., "Fast and effective optimization of arrays of submerged wave energy converters." in *2016 Proceedings of the Genetic and Evolutionary Computation Conference (GECCO)*, Denver, USA, Jul. 2016, pp. 1045-1052.
[32] A. Garcia-Teruel and D. I. M. Forehand, "A review of geometry optimisation of wave energy converters," *Renewable and Sustainable Energy Reviews*, vol. 139, Apr. 2021.
[33] Z. He, D. Ning, and Y. Gou *et al*., "Optimization of a wave energy converter square array based on the differential evolution algorithm," *Ocean Engineering*, vol. 262, Oct. 2022.
[34] D. Golbaz, R. Asadi, and E. Amini *et al*., "Layout and design optimization of ocean wave energy converters: a scoping review of state-of-the-art canonical, hybrid, cooperative, and combinatorial optimization methods," *Energy Reports*, vol. 8, pp. 15446-15479, Nov. 2022.
[35] E. Simley, N. Angelou, and T. Mikkelsen *et al*., "Characterization of wind velocities in the upstream induction zone of a wind turbine using scanning continuous-wave lidars," *Journal of Renewable & Sustainable Energy*, vol. 8, Jan. 2016.
[36] W. Zhao, L. Wang, and Z. Zhang, "Artificial ecosystem-based optimization: a novel nature-inspired meta-heuristic algorithm," *Neural Computing and Applications*, vol. 32, pp. 9383-9425, Sep. 2019.
[37] W. Zhao, Z. Zhang, and L. Wang, "Manta ray foraging optimization: an effective bio-inspired optimizer for engineering applications," *Engineering Applications of Artificial Intelligence*, vol. 87, Jan. 2020.

[38] H. Esmaeil, P. Saeid, and G. Hassan *et al.*, "Power absorption of combined wind turbine and wave energy converter mounted on braceless floating platform," *Ocean Engineering*, vol. 266, Dec. 2022.
[39] M, Hansen and H. A. Madsen, "Review paper on wind turbine aerodynamics," *Journal of Fluids Engineering*, vol. 133, no. 11, Nov. 2011.
[40] J. N. Sorensen, "Aerodynamic aspects of wind energy conversion," *Annual Review of Fluid Mechanics*, vol. 43, no. 1, pp. 427-448, Jan. 2011.
[41] R. G. Hamid, G. Hassan, and A. Alireza *et al.*, "Novel concept of hybrid wavestar-floating offshore wind turbine system with rectilinear arrays of WECs," *Ocean Engineering*, vol. 266, Oct. 2022.
[42] M. R. Pau, N. Vincenzo, and B. R. T. Mathew *et al.*, "Layout optimization of wave energy converter arrays," *Energies*, vol. 10, no. 1067, pp. 1-17, Jul. 2017.
[43] B. Child and V. Venugopal, "Optimal configurations of wave energy device arrays," *Ocean Engineering*, vol. 37, no. 16, pp. 1402-1417, Nov. 2010.
[44] D. Sarkar, E. Contal, and N. Vayatis *et al.*, "Prediction and optimization of wave energy converter arrays using a machine learning approach," *Renewable Energy*, vol. 97, pp. 504-517, Nov. 2016.
[45] K. Ezhilsabareesh, R. Suchithra, and A. Samad, "Performance enhancement of an impulse turbine for OWC using grouped grey wolf optimizer based controller," *Ocean Engineering*, vol. 190, Oct. 2019.
[46] A. Ramadan, S. Kamel, and M. M. Hussein *et al.*, "A new application of chaos game optimization algorithm for parameters extraction of three diode photovoltaic model," *IEEE Access*, vol. 9, pp. 51582-51594, Mar. 2021.
[47] F. A. Hashim, E. H. Houssein, and K. Hussain *et al.*, "Honey badger algorithm: new metaheuristic algorithm for solving optimization problems," *Mathematics and Computers in Simulation*, vol. 192, pp. 84-110, Mar. 2021.